ADVANCED FUNCTIONAL MATERIALS
www.afm-journal.de

Materials Views
www.MaterialsViews.com

A Non-Mulberry Silk Fibroin Protein Based 3D In Vitro Tumor Model for Evaluation of Anticancer Drug Activity

*Sarmistha Talukdar and Subhas C. Kundu**

The limitations of clinical chemotherapy are credited primarily to drug resistance. Effective development and screening of new drugs require appropriate in vitro tumor models that resemble the in vivo situation to evaluate drug efficiency and to decrease the use of experimental animals. 3D in vitro model systems that are able to mimic in vivo microenvironments are now highly sought after in cancer research. Here, the characteristics of breast cancer cell line MDA-MB-231 cells on 3D, and 2D *Antheraea mylitta* silk matrices and tissue culture plates are compared. After long term culture of breast cancer cells in the silk scaffold, the engineered tumor construct shows different zones of cell proliferation, such as an avascular tumor. Silk fibroin matrix 3D tumor models are studied for the evaluation of various anticancer drugs. The cytotoxic effects of three different drugs (Paclitaxel, Celecoxib, and ZD6474) at different concentrations are evaluated for MDA-MB-231 grown on 2D films as well as on a 3D fibroin scaffold. Higher drug concentrations are required to achieve a comparable reduction in cell viability and invasive potential in 3D culture. Combinatorial treatment of drugs at IC_{50} concentrations result in up to 84% death of cancer cells. The results indicate that 3D in vitro tumor models may be better systems to evaluate cancer treatment strategies.

1. Introduction

Tissue engineering has provided a major impact on regenerative medicine and its applications for personalized medicine. Tissue engineering approaches may have an equally significant impact on cancer medicine.[1] Cancer is a disease whose story is yet to be clearly unfolded. It involves numerous factors, genes and their interplay in cancer initiation and progression. 2D cell culture techniques have tremendously helped in interpreting advancing our knowledge on complex biological phenomena. However, from both anatomical and physiological aspects, cancer cells in vivo are under the influence of a 3D microenvironment characterized by several factors differentiating them from cancer cells grown in monolayer.[2–4] For example, in a 2D culture, the cancer cells are cultured in a single layer, in nutrient and oxygen rich environment, with very limited contact with neighbouring cells. There are some other limitations of 2D cell culture experiments, such as different physiological patterns of cell adherence, cytoskeletal organization, cell migration, signal transduction, morphogenesis, proliferation, differentiation and response to drugs.[6–10] There is a substantial body of work, which describe the impact of all of these microenvironmental factors on cancer cells.[11–15] In real life most cancer cells form a 3D tumor mass, closely contacting and interacting with one another, poorly supplied with nutrients and oxygen.[16] The complex biological phenomena involved in the 3D tumor microenvironment play a very determining role in several of its phenotype, including resistance to drugs.[17–19] Initially it was thought that the drug resistance of 3D in vitro tumors was due to poor diffusion of the drugs to interior cells but now it has been proved that mere inaccessibility to nutrients cannot account for this phenomenon[20] This shows how important it is to consider the microenvironment in the design and evaluation of new anticancer drugs. But the importance of these factors have been largely ignored by cancer researchers and pharmaceutical and biomedical industries[21] 3D culture assays provide a useful platform for dissecting these processes[22–25] as well as applying them for evaluation of new drugs. 3D tumor models may bridge the gap between traditional 2D cell-culture methods and expensive and labour-intensive animal models.[4,11,21] There is no universal treatment for cancer, as there are several different types of cancer, each with its different pattern of gene expression and progression. Differences exist even in cancer patients of the same type of cancer. This presents a need for development of therapeutic strategies to treat cancer effectively and clinically appropriate 3D in vitro tumor models may act as effective tools for drug evaluation. Development of such highly complex models initially require engineering and evaluation of pilot models which can be further tailored for futher investigations. Modeling of avascular tumors is a first step toward building models for advanced tumors.[16] Such in vitro 3D tissue models may fulfill the need for reductionist approaches to understand in vivo molecular mechanisms.[4]

Among the numerous factors involved in cancer initiation, growth and progression, a few extensively studied are protein kinase C (PKC), matrix metalloproteinases (MMPs), Vascular endothelial growth factor (VEGF) and interleukin 8 (IL-8). PKC is a family of serine-threonine kinases, which play an important role in cancer cell proliferation, migration, adhesion

S. Talukdar, Prof. S. C. Kundu
Department of Biotechnology
Indian Institute of Technology
Kharagpur 7213 02, India
E-mail: kundu@hijli.iitkgp.ernet.in

DOI: 10.1002/adfm.201200375

and malignant transformation. Its isoforms have activities like increased cancer cell motility and invasion, induced proliferation, suppression of apoptosis, and mediating angiogenesis.[26] The influence of PKCs in cancer emanates from their function as receptors for tumor promoting agents or as downstream targets of growth factor receptors.[26] Expression of various MMPs has been found to be up-regulated virtually in every type of human cancer and correlates with advanced stage, invasive and metastatic properties and, in general, poor prognosis.[27–30] MMPs influence many areas of tissue function by degrading extracellular matrix (ECM), cell adhesion and cell surface receptors and regulating the bioavailability of many growth factors and chemokines.[29,31,32] Improper regulation of MMPs can contribute to the cancer pathogenesis.[33,34] Among these different MMPs, MMP-9 is the key enzyme for degrading type IV collagen, a major constituent of the ECM. MMP-9 also influences tumor angiogenesis by increasing the availability of VEGF[34] a key player in tumor angiogenesis. VEGF along with IL-8 are useful diagnostic factors for overall survival in cancer patients.[35] Increased occurrence of such pro-angiogenic factors is linked with aggressive tumor growth and decreased patient survival.[36,37] VEGF and IL-8 are potent pro-angiogenic factors secreted by cancer cells, which help in development of tumor neovasculature.[37] Additionally VEGF also promotes breast cancer cell survival and invasiveness.[38,39] IL-8 has several functions that promote tumor growth, motility and metastasis.[40]

Inhibitors of these proteins and their receptors applied in basic cancer research as well as in clinical trials. ZD6474 is an inhibitor of VEGF receptor-2 kinase and EGF receptor tyrosine kinase activity.[41] Celexocib another cancer treating drug acts through selective non-competitive inhibition of COX-2.[42] These drugs are able to affect several signaling pathways involved in cancer growth and progression. Celecoxib treatment also decreases the expression of VEGF and MMP-9[43] suggesting a possible mechanism in inhibition of angiogenic pathways. ZD6474 is also potent inhibitor of RET receptor tyrosine kinase activity, thereby maybe capable of causing additional antitumor effects.[41] Apart from these pathway inhibitors mitotic inhibitors are also used for chemotherapy, one of the most commonly used is Paclitaxel. Paclitaxel binds to tubulin heterodimer,[43] interfering with microtubule breakdown and arresting cell division. Extensive studies have been undertaken using various cell lines to understand to evaluate and understand the molecular mechanism of activity of all these drugs.

For the evaluation of any anti-cancer drug it is important to study the effect it has on the activity of above mentioned proteins, along with other proteins which are intricately involved in carcinogenesis. Chemotherapy drugs are most effective when administered in combination (combination chemotherapy). The rationale for combination chemotherapy is to utilize drugs that target different molecules involved in cancer, targeting different mechanisms of action, thereby decreasing the chances of development of drug-resistant cancers. When drugs with different effects are combined, each drug can be used at its least effective dose, resulting in decrease of associated side effects. Before any combination of drugs are used, it is essential to study whether there are any inter-drug interactions and what positive or negative impact it can offer when administered. This requires a clinically accurate platform where tumor cells can grow, proliferate and express as the cells do in vivo. In vitro tumor models can play a major role in the discovery of effective chemotherapeutic systems. Attention to engineering principles can lead to the design of more complex, but more robust, models.[44]

Recently we have reported the growth of human breast adenocarcinoma MDA-MB-231 cell lines on 3D porous silk fibroin scaffold.[45] Our hypothesis was 3D in vitro silk scaffold based tumor would provide better information on the morphology, proliferation and metabolic activities of breast cancer cells than the standard 2D culture techniques. Non-mulberry *A. mylitta* silk fibroin protein scaffolds provide a suitable, biocompatible, 3D microenvironment for cancer cell attachment, growth and tissue formation and can perform as an in vitro tumor model.[45] The protein has been found conducive for the growth of several cells such as fibroblasts, human mesenchymal stem cells and rat bone stromal cells, and differentiation into osteocytes and adipocytes.[46–48] Here we study this silk fibroin based 3D in vitro tumor model for evaluation of anticancer drug activity of Paclitaxel, Celecoxib and ZD6474. This system enabled us to show that long-term cultures of cancer cells in silk scaffolds reflects the physical, biological, and biochemical microenvironment of cancer in vivo. Expression of VEGF, IL-8, PKC and MMP-9 is much higher in 3D cultures than in 2D cultures. Significantly higher drug concentrations are required to achieve comparable reduction in cell viability and invasive potential in 3D culture than 2D cultures.

2. Results and Discussion

2.1. Cytocompatibility of MDA-MB-231 Cells Grown on TCP, 2D Films, and 3D Matrices

2D films and 3D scaffolds were fabricated (**Scheme 1**), as reported by our group previously MDA-MB-231 cells were grown on 2D and 3D matrices and samples were taken after 1, 3, 5, 7, 9, 11, 13 and 15 days of growth intervals to monitor cell growth (**Figure 1**). The first peak cell growth was observed on Day 5 on the 2D matrices. Reduction in cell growth as observed on day 7, 11 and 15 due to confluence. It was also observed that after attaining maximum confluence, the viability of cells falls, and the dead cells float away from the matrix creating space for the remaining viable cells to grow. The growth again increases on day 9 and 13 as the remaining cells proliferate on the available area. Highest growth in 3D culture, was obtained on day 15. The overall growth profile observed in 3D cell culture was higher than that achieved in the 2D. In our earlier work we observed that 3D cancer culture on scaffolds also follows the Gompertz law of cancer growth.[49] The results may be explained by the fact that signaling and other cellular functions differ in three-dimensional compared with two-dimensional systems. Cell adhesion structures can evolve in vitro towards in-vivo-like adhesions with distinct biological activities.[17] Growth pattern comparisons indicate that 3D silk scaffold is probably more suitable for long term growth of MDA-MB-231 breast cancer cells in vitro.

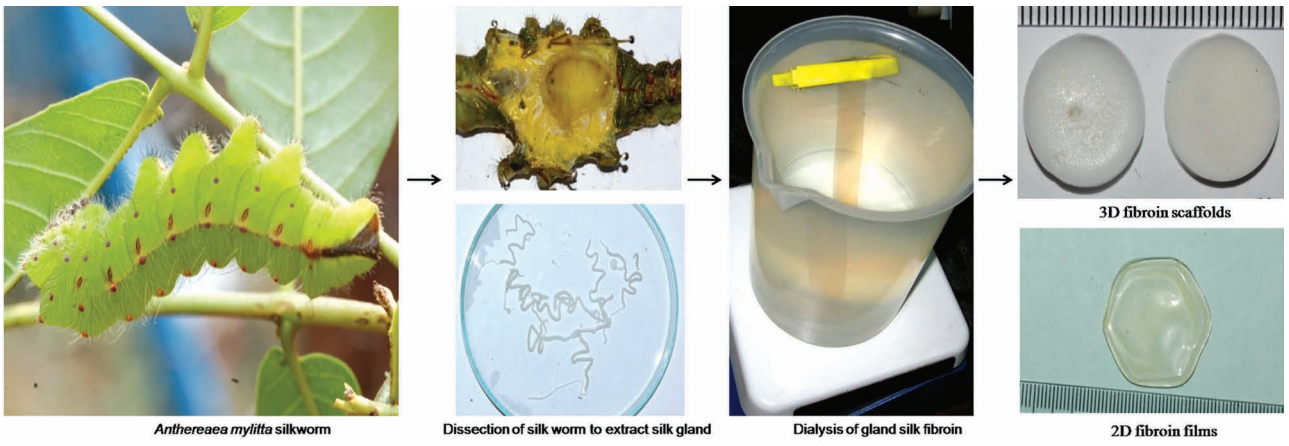

Scheme 1. Schematic representation of the preparation of scaffolds and films of fibroin isolated from silk gland of non-mulberry tropical silkworm *A. mylitta*. Silkworms were dissected to extract silk glands. Fibroin was carefully isolated from the glands and dialyzed to obtain silk fibroin solutions. The solution was used to fabricate scaffolds and films.

2.2. Morphology of MDA-MB-231 Cells in Long Term Culture on *A. mylitta* Fibroin Scaffolds

The scaffold took the Hoechst 33342 stain, demonstrating distinct pore boundaries throughout the scaffold surface. Rhodamine-phalloidin and Hoechst 33342 staining of *A. mylitta* fibroin scaffolds seeded with MDA-MB-231 cells showed the presence of well defined actin cytoskeleton and nucleus in all the cells. Z-sectioning of the seeded scaffolds showed presence of cells in topmost as well as inner sections. But the highest number of cells were observed in the outermost peripheral region and decreased towards the center (**Figure 2**). This indicates that the tumor construct in long term 3D culture may show characteristics of an avascular tumor spheroid. An avascular tumor is composed of outermost proliferating zone, inner quiescent zone and central necrotic core. The nutrient concentration at the center decreases due to consumption, as it diffuses away from the blood vessel, which may cause the cells at the central core to die[16] Diffusion and nutrient consumption may limit tumor growth, and earlier studies have described the spatio-temporal interactions between tumor cell populations and nutrients[16,50] and calculated the nutrient and oxygen concentration profiles as a function of tumor spheroid radius that was changing due to the rate of cell proliferation.[16,50] They reported that at the edges of vthe tissue the oxygen concentration matches that within the solution surrounding the tissue (Michaelis-Menten form of oxygen consumption) and that the oxygen and glucose concentrations will decrease in the middle of the spheroid, resulting in a significantly reduced rate of proliferation.[50,51] This may give rise to a region of high cell proliferation near the edge of the spheroid, and a core region of dead cells. Their model also predicts that the pH inside the tumor spheroid should be different from that in the external medium, with higher acidity at the tumor center than near the tumor boundary and this has also been confirmed experimentally.[50] In our earlier work we observed that 3D culture is more appropriate for long term growth.[49] We had found that growth of cancer cells in 3D scaffolds follows the Gompertz law of tumor

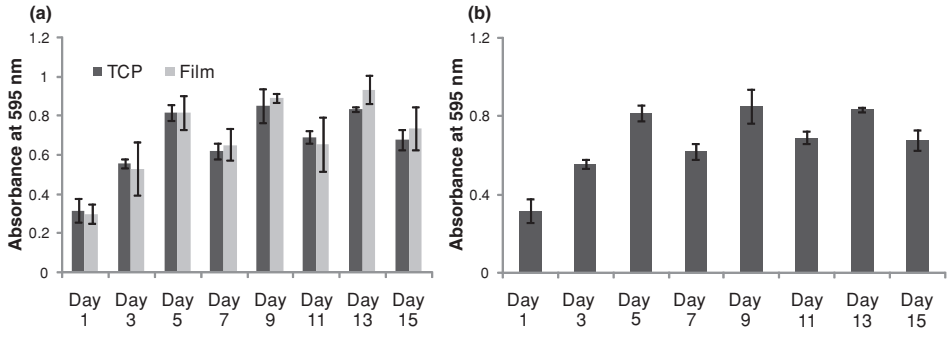

Figure 1. Cytocompatibility of MDA-MB-231 breast adenocarcinoma cells grown on a) TCP and 2D silk films and b) 3D silk matrices by MTT assay. Each point represents the mean from three independent experiments. The peak cell growth was observed on day 5 on the 2D matrices after which decrease in cell growth as observed on day 7, 11 and 15 due to confluence. Cell proliferation was observed to be higher in 3D cells with the highest growth on day 15. The error bars denote ± SD (standard deviation for n = 3).

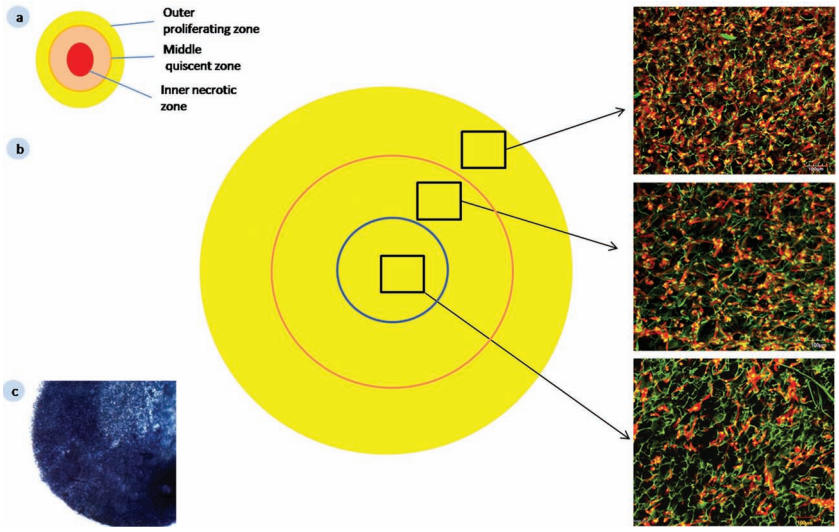

Figure 2. a) Schematic representation of an avascular tumor spheroid model showing its areas of cell growth. b) Confocal laser microscopy image showing the distribution of MDA-MB-231 cells throughout the various regions of the in vitro tumor model. The highest number of cells were observed in the outermost peripheral region and decreased towards the center. Scale bars represent 100 µm. c) Tumor construct stained with trypan blue showing distribution of the dye.

growth kinetics, but not in 2D cultures of same cell density and culture duration. In the present study, scaffold seeded with high density of cells (3×10^6 cells) and grown for 60 days within the 3D confined space of the scaffold (Figure 2b), the cells may face similar competition and depletion of nutrients and oxygen as the tumor spheroids, leading to formation of similar zones of proliferation. The tumor construct relies on diffusion from the surrounding media for supply of oxygen, nutrients and removal of waste products. As the tumor grows, nutrient demand increases until the flux of nutrients through the surface of the tumor construct is too small to supply the entire mass of cells.

2.3. Trypan Blue Diffusion in Tumor Constructs

Tumor constructs were stained with Trypan Blue dye to visualize the diffusion of media and drugs into the tumor constructs. Trypan blue was used as this dye is not taken up dead cells and has been used as a model drug by researchers. Darker stains were observed in the peripheral region, than the central core region. The result suggests that diffusion of media and drugs into the tumor constructs follows a gradient, with the peripheral regions having similar concentration as the surrounding solution, and this concentration decreases towards the center.

2.4. Determination of IC_{50} of Anticancer Drugs

Cell inhibition studies were carried out with different drug concentrations and compared for both 2D and 3D cell cultures. From **Figure 3** it can be observed that for 2D cultures, 7.5 ± 0.34 µM of Paclitaxel, or 344.5 ± 0.03 µM of Celeoxib or 6.57 ± 0.09 µM of ZD6474 drug concentration needed to reduce cell growth by half. For 3D culture the IC_{50} concentration for Paclitaxel, Celeoxib and ZD6474 was 50 ± 0.17 µM, 934.02 ± 0.21 µM, 25 ± 0.04 µM respectively. This shows that higher concentration of drug is needed in MDA-MB-231 cancer cells grown in 3D than those in 2D.

The number of cells in 3D scaffolds is more than that in 2D cultures. The increased resistance could be because of

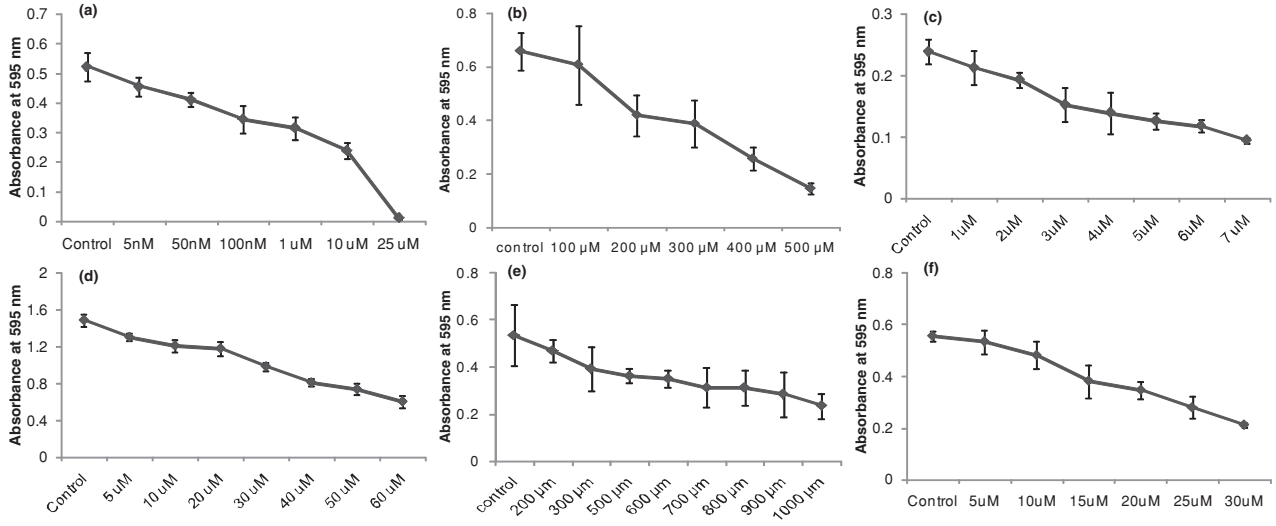

Figure 3. Viability of MDA-MB-231 cells treated with anticancer drugs and determination of their IC_{50} concentrations. The cells were grown for 7 days before treatment. a) Paclitaxel on cells cultured on 2D films, b) Celecoxib on cells cultured on 2D films, c) ZD6474 on cells grown on 2D films, d) Paclitaxel on cells grown in 3D scaffolds, e) Celecoxib on cells grown in 3D scaffolds, and f) ZD6474 on cells grown in 3D scaffolds (n = 3). The error bars denote ± SD (standard deviation for n = 3).

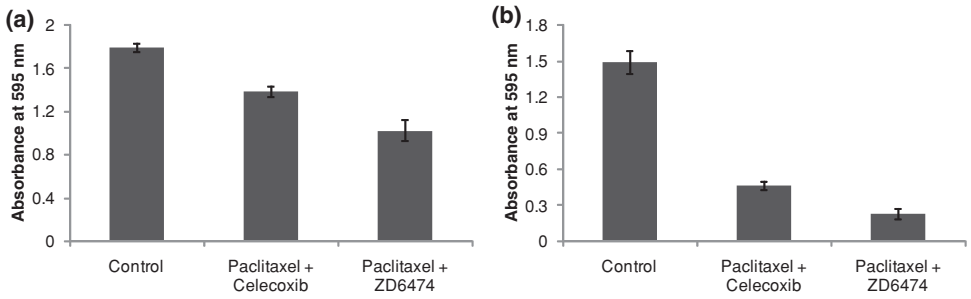

Figure 4. Viability of MDA-MB-231 cells treated with anticancer drugs. a) Cells cultured on 2D films untreated or treated with Paclitaxel (7.5 μM) and Celecoxib (344.5 μM) or Paclitaxel (7.5 μM) and ZD6474 (6.57 μM). b) Cells grown in 3D scaffolds (n = 3) untreated or treated with combination of Paclitaxel (50 μM) with Celecoxib (934 μM) and combination of Paclitaxel (50 μM) with ZD6474 (25 μM). Treating cells with combination of Paclitaxel (7.5 μM) and Celecoxib (344.5 μM) or Paclitaxel (7.5 μM) and ZD6474 (6.57 μM) resulted in of 77.4% and 47.3% cell viability, respectively. When treated with the higher concentrations of Paclitaxel (50 μM) and Celecoxib (934 μM) or Paclitaxel (50 μM) and ZD6474 (25 μM), increased cytotoxicity was observed with the combination of Paclitaxel and ZD6474 proving to be more cytotoxic than the other combinations. The error bars denote ± SD (standard deviation for n = 3, $P < 0.05$, * represent significant statistical difference and $P < 0.01$ represent highly significant difference).

presence of more number of cells. Since, the drug is solubilized in the media, and the media is unable to diffuse uniformly in the densely cell populated 3D cultures. Therefore, all the cells of 3D cultures may not be available to interact with the drug. Also, from both anatomical and physiological aspects, cancer cells in vivo are under the influence of a 3D microenvironment characterized by several factors differentiating them from cancer cells grown in monolayer.[2–4] For example, in a 2D culture, the cancer cells are cultured in a single layer, in nutrient and oxygen rich environment, with very limited contact with neighboring cells. While in real life most cancer cells form a three-dimensional tumor mass, closely contacting and interacting with one another, poorly supplied with nutrients and oxygen. The complex biological phenomena involved in the tumor microenvironment play an important role in determining several of its phenotype including resistance to drugs.[5,52] Several reports have emphasized on the role of 3D culture on increased drug resistance.[5,53,54] Phenotypical differences between normal and malignant epithelial breast cells have been observed exclusively in 3D.[12,55,56] The mechanism of elevated chemoresistance to anti-cancer reagents has also been attributed to decreased penetrance of anti-cancer drugs, increased pro-survival signalling, and/or upregulation of genes conferring drug resistance,[55] increased compaction and intercellular adhesion in 3D cell aggregates.[57] Such 3D cell aggregates often result in hypoxia in the tumor center and interactions between cell and ECM may also alter response to drugs.[57] Several factors are involved in the phenomenon of increased resistance to drugs, and it may be useful to consider the microenvironment in the design and evaluation of new anticancer drugs. 3D culture assays may therefore prove as useful tools for evaluation of new drugs.

2.5. Cytotoxic Assay of Treated and Untreated Cells

Combinatorial drug evaluation was done on 3D scaffolds seeded with 10^6 cells seeded and grown for 15 days. Combinations of two drugs at different concentrations were carried out. One set of scaffolds were treated to drug concentrations that had killed half the population of cells in 2D, i.e., combinations of Paclitaxel (7.5 μM) and Celecoxib (344.5 μM) or Paclitaxel (7.5 μM) and ZD6474 (6.57 μM). Another set of scaffolds were treated to drug concentrations that had killed half the population of cells in 3D, i.e., combinations of Paclitaxel (50 μM) and Celecoxib (934 μM) or Paclitaxel (50 μM) and ZD6474 (25 μM). The cell viability of these sets was compared to that of untreated cells. Treating cells with combination of Paclitaxel (7.5 μM) and Celecoxib (344.5 μM), Paclitaxel (7.5 μM) and ZD6474 (6.57 μM) resulted in of 77.4% and 47.3% cell viability respectively (**Figure 4**). When treated with the higher concentrations of paclitaxel (50 μM) and Celecoxib (934 μM) or Paclitaxel (50 μM) and ZD6474 (25 μM), cytotoxicity of 68.8% and 84.5%. The combination of Paclitaxel (50 μM) and ZD6474 (25 μM) seem to be more cytotoxic than the other combinations (Figure 4).

2.6. Cell Viability Assay

To study the biocompatibility of the matrices as potential biomaterials, we performed live/dead assays (Molecular Probes). Cell viability was observed using confocal microscopy. Decrease in the number of viable cells was observed in the drug treated samples, the least being the constructs treated with paclitaxel (50 μM) and ZD6474 (25 μM). The number of live cells was maximum in untreated constructs, followed by the constructs treated with Celecoxib (934 μM), Paclitaxel (50 μM), ZD6474 (25 μM), combinations of Paclitaxel (50 μM) and Celecoxib (934 μM) and Paclitaxel (50 μM) with ZD6474 (25 μM). The drug treated live cells were smaller in size with unhealthy cell morphology (**Figure 5**). Cell size is a fundamental and easily observable aspect of cell phenotype. Loss of cell volume or cell shrinkage, termed apoptotic volume decrease (AVD) is often an indicator of apoptosis.[58]

2.7. MMP-9 Activity of MDA-MB-231 Cells on Silk Scaffolds

Matrix metalloproteinases play an important role in tumor proliferation, survival, migration angiogenesis and tumor aggressiveness. MMPs function by degrading the ECM to aid in

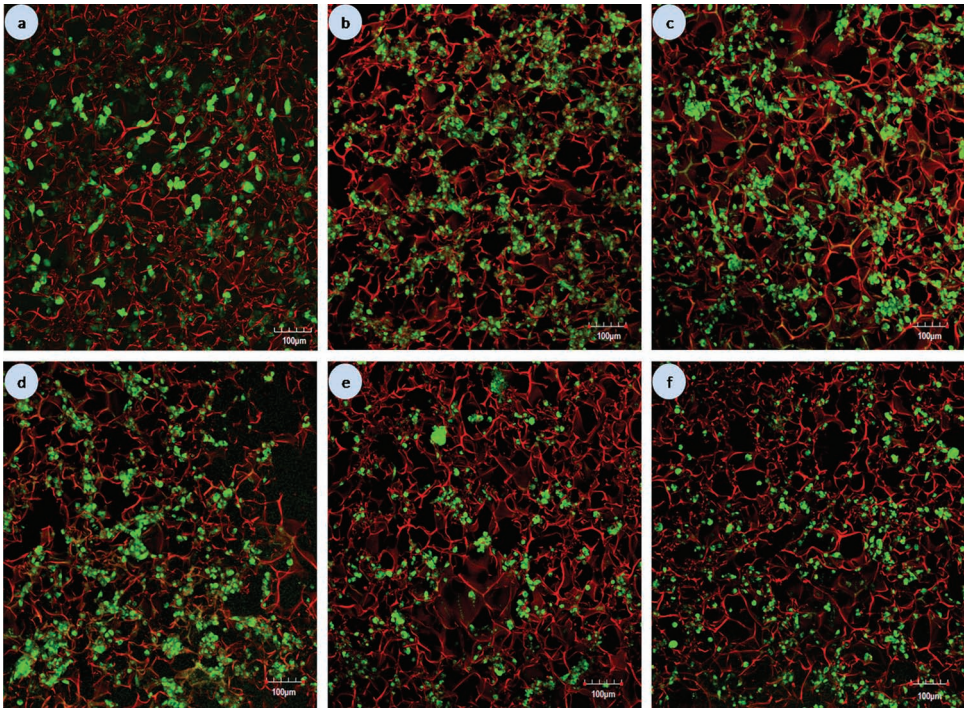

Figure 5. Live/dead stained confocal microscopy images showing MDA-MB-231 breast adenocarcinoma cell attachment, morphology and viability on: a) untreated constructs and b) constructs treated with Paclitaxel (50 μM), Celecoxib (934 μM), ZD6474 (25 μM), a combination of Paclitaxel (50 μM) with Celecoxib (934 μM), and a combination of Paclitaxel (50 μM) with ZD6474 (25 μM). The drug treated live cells, which can be visualized in green, were smaller in size with unhealthy cell morphology compared to the untreated cells. Images were taken from the mid-peripheral region of the constructs in all the cases. Scale bars represent 100 μm.

cancer invasion and create a favourable tumor microenvironment. MMP-9 also increases the availability of VEGF and thus regulates angiogenesis. Increased levels of MMP-9 and MMP-2 are found in the serum and plasma of patients suffering from breast cancer.[59] MMP-9 activity was determined by area, perimeter and intensity of the bands. MMP-9 activity was highest in cells cultured without drugs. Least MMP-9 activity was shown by cells treated with combinations of Paclitaxel (50 μM) with Celecoxib (934 μM), and ZD6474 (25 μM) (**Figure 6**).

2.8. Angiogenic Activity of MDA-MB-231 Cells on 2D and 3D Matrices

Use of combinations of drugs lowered the production of VEGF. IL-8 production was not drastically effected by the usage of IC_{50} drugs concentrations optimized for 2D culture. The IC_{50} drug concentrations optimized for 3D culture were more effective than those optimized for 2D cultures for lowering the production of both VEGF and IL-8. The most effective was the combination of Paclitaxel (50 μM) and ZD6474 (25 μM) (**Figure 7**).

2.9. Morphology of Treated and Untreated Cells

Rhodamine-phalloidin and Hoechst 33342 staining was carried out to observe the cell morphology and number of cells in the scaffolds. Both treated and untreated constructs showed the presence of well defined cytoskeleton and nucleus in all the cells (**Figure 8**). The scaffold stained with Hoechst 33342 showed well defined pores. Z-sections of the seeded scaffolds were attacked to obtain the complete distribution of cells at a particular microscopic field. Staining of both cells and scaffold helped in showing distribution of the cells within the pores under treated and un-treated conditions. The distribution of cancer cells in untreated conditions was more than those treated with the anticancer drugs.

2.10. Immunostaining

Protein kinase C (PKC) is a family of serine-threonine kinases which control cell proliferation, migration, adhesion, malignant transformation, increased motility, invasion and angiogenesis.[26] A positive correlation has been determined between elevated PKC levels and both the invasive and chemotactic potential of human breast cancer cell lines.[60] Their role stems from their functions as receptor for tumor promoting agents or as downstream targets of growth factor receptor.[26] PKC β, an isoform, controls VEGF mediated neovascularization of tumor.[61] Multiple PKC isoforms control the expression and activity of MMP-9.[62] Immunostaining of constructs against PKC revealed comparatively higher expression of PKC localized in the nuclei of untreated tissue constructs. PKC was visualized as pink

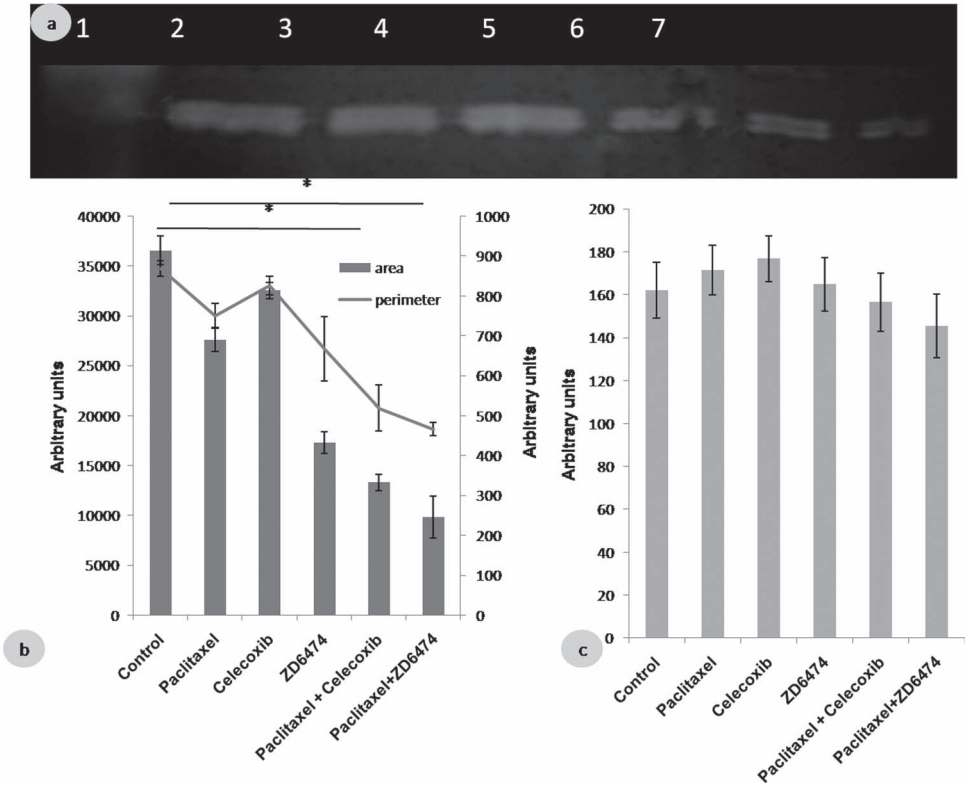

Figure 6. Gelatinase zymography of conditioned media from drug treated and untreated samples. a) Zymogram with Lane 1: Collagenase (Positive control); Lane 2: untreated; Lane 3: 2D treated with Paclitaxel (50 μM); Lane 4: treated with Celecoxib (934 μM); Lane 5: treated with ZD6474 (25 μM); Lane 6: treated with Paclitaxel (50 μM) and Celecoxib (934 μM); and Lane 7: treated with Paclitaxel (50 μM) and ZD6474 (25 μM). b) Mean area and perimeter and c) mean intensity of the bands in arbitrary units, as analyzed using Image J (NIH) software. The least MMP-9 activity was shown by cells treated with combinations of Paclitaxel with Celecoxib and ZD6474. The error bars denote ±SD (standard deviation for $n = 3$, $P < 0.05$, * represent significant statistical difference).

areas within the blue nuclei. In the drug treated samples PKC expression per nuclear area was found to be lower (**Figure 9**). This may be in concordance with the results obtained by gelatinase zymography. The nuclei of untreated samples were also observed to be comparatively larger than the drug treated samples. This may be due to the breakage of nucleus into chromosomal bodies during apoptosis. Inhibition of PKC is also known to cause apoptosis. In the future, it will be important to further investigate how different drugs will affect cell behavior in the different regions, to understand the potential of silk based tumor constructs.

3. Conclusions

Based on our earlier findings,[49] we have evaluated the efficacy of various concentrations and combinations of anti-cancer drugs on our in vitro 3D tumor model. The concentrations required for 50% cell death in 3D cultures was much more than that in 2D cultures. Combinations of anti-cancer drug caused lower percentages of cell viability in 3D. The most effective was the combination of Paclitaxel (50 μM) and ZD6474 (25 μM) causing 84.5% of cell death. Higher drug concentrations and their combinations were able to decrease the expression of VEGF, IL-8, PKC and MMP-9 significantly. Marked changes were noticed in live cell size, nuclear size and cell morphology. The changes are possibly due to drug mediated apoptosis. The results indicate that in vitro 3D tumor model may be used for evaluating new drugs. 3D interactions between cells and ECM may allow malignant morphologies to develop in a more realistic context.[57] A number of parameters are needed to build the models for specific experimental conditions.

4. Experimental Section

Preparation of Fibroin from A. mylitta Silkworm: *A. mylitta* silk fibroin was prepared as described in our earlier reports.[49,63] The glands were washed with distilled water to remove the traces of sericin and the protein was squeezed out of the gland with the help of fine forceps. The silk fibroin protein isolated from the gland was either used immediately or was stored at –20 °C till further use. The frozen silk gland fibroin protein was used by thawing at room temperature. Both the fresh or thawed silk fibroin protein can be dissolved in 1% (w/v) SDS aqueous solution containing 10 mM Tris (pH 8.0) and 5 mM EDTA at room temperature. The solution obtained was dialyzed (MWCO 12000) to remove the excess SDS and regenerated aqueous 2% (w/v) silk fibroin solution was achieved. Fibroin solution was collected and the concentration was determined by weighing the remaining solid mass after drying at 60 °C.

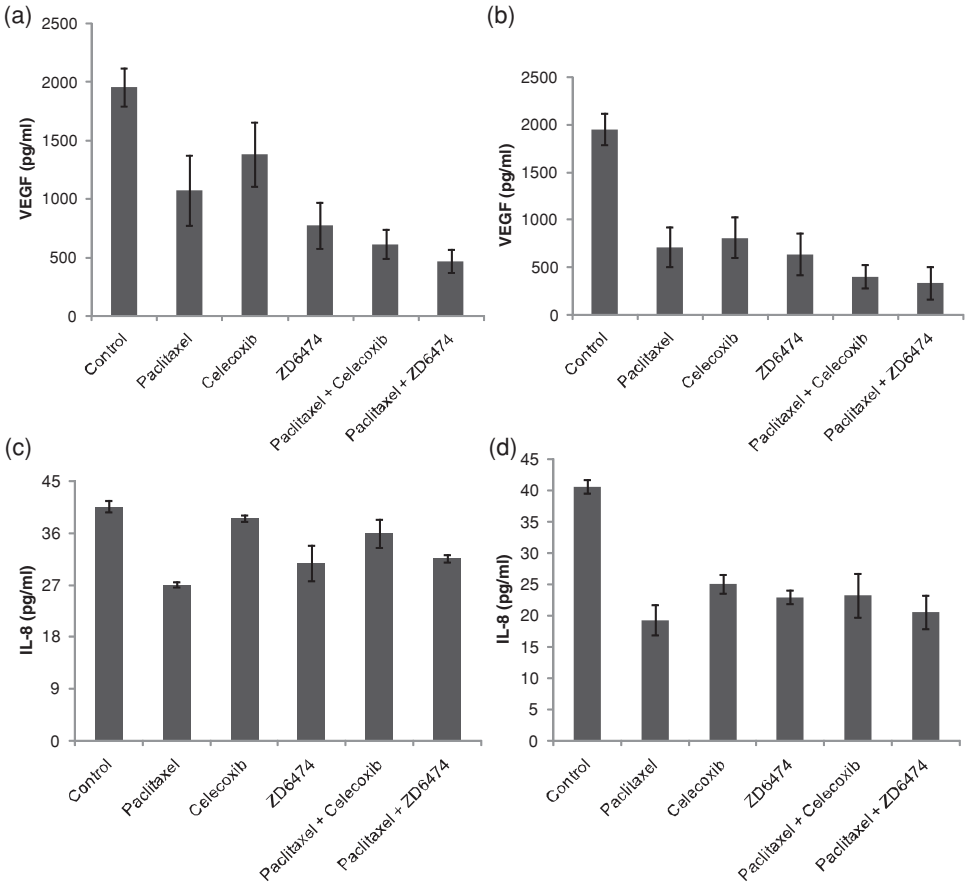

Figure 7. Production of VEGF by MDA-MB-231 cells treated with anticancer drugs. a) Cells cultured on 2D films treated or untreated with Paclitaxel (7.5 μM), Celecoxib (344.5 μM), ZD6474 (6.57 μM), and their respective combinations. b) Cells grown in 3D scaffolds (n = 3) treated with Paclitaxel (50 μM), Celecoxib (934 μM), ZD6474 (25 μM), a combination of Paclitaxel (50 μM) with Celecoxib (934 μM), and a combination of Paclitaxel (50 μM) with ZD6474 (25 μM). Production of IL-8 by MDA-MB-231 cells treated with anticancer drugs. Cells cultured c) on 2D films and d) on cells grown in 3D scaffolds (n = 3) treated with Paclitaxel (50 μM), Celecoxib, ZD6474 (25 μM), a combination of Paclitaxel (50 μM) with Celecoxib, and a combination of Paclitaxel (50 μM) with ZD6474 (25 μM). The most effective for reducing VEGF and IL-8 secretion was the combination of Paclitaxel and ZD6474. The error bars denote ±SD (standard deviation for n = 3, $P < 0.05$, * represent significant statistical difference).

Preparation of Fibroin Films: The 2% (w/v) fibroin isolated from *A. mylitta* gland was passed through a filter with a pore size of 0.22 μm. These films were cast onto the surfaces of 12-well tissue culture plates (TCP). The plates were kept under laminar flow for 6–8 h for drying, and the films were treated with 70% ethanol and then washed with phosphate buffered saline. UV-treatment was done for 20 mins. to sterilize the films. They were then blocked using 0.02% BSA in sterile phosphate buffered saline for 30 min and the excess BSA was removed by washing three times in phosphate buffered saline. These silk fibroin film-coated culture plates were then used in further cell culture studies.[49]

Preparation of Porous Fibroin Scaffolds: The 2 wt% (w/v) fibroin solutions from *A. mylitta* gland solution were put into moulds and then frozen at −20 °C for 8 h. These were then lyophilized to yield a porous matrix. The porous matrices were immersed in ethanol to induce *β*-sheet crystallization and insolubility in water. The insoluble fibroin 3D scaffolds were washed with PBS at room temperature and sterilized by UV treatment and were then used for cell culture studies.[49,63] The final scaffold dimensions obtained were of 13.5 mm diameter by 2.5 mm thickness.

Cell Culture, Maintenance, and Seeding of Breast Cancer Cells in Silk Scaffolds and Films: MDA-MB-231 cell line was cultured in DMEM medium with 10% FBS. Confluent monolayer was washed with sterile phosphate-buffered saline (PBS) and split by treatment 0.05% trypsin/EDTA solution. The culture medium was replaced every 3 days. Scaffolds and films were sterilized by immersion in 70% ethanol for 1 h. This was followed by rehydration in sterile phosphate-buffered saline (PBS). Cells were trypsinized counted with help of a haemocytometer and 10^5 cells were seeded on 24-well plates containing *A.mylitta* fibroin scaffolds. The required number of cells were suspended in a volume of 20 μl. 10 μl of this suspension was seeded on the top surface of the scaffolds, with 2 μl at 4 peripheral points, and 2 ul at the central point. These cells were allowed to attach for a 3 hours at 37 °C and 5% CO_2. The scaffolds were turned over and the rest of 10 μl suspension was seeded in a similar fashion.

Trypan Blue Diffusion Staining: MDA-MB-231 cell line was cultured in DMEM medium with 10% FBS. Confluent monolayer was washed with sterile phosphate-buffered saline (PBS) and split by treatment 0.05% trypsin/EDTA solution. The culture medium was replaced every 3 days. Scaffolds and films were sterilized by immersion in 70% ethanol for 1 h. This was followed by rehydration in sterile phosphate-buffered saline (PBS). 2×10^6 cells were seeded on 24-well plates containing *A. mylitta* fibroin scaffolds (5 mm in diameter and 2 mm in thickness) and grown for 14 days. The scaffolds were then stained with Trypan Blue for 1 h and

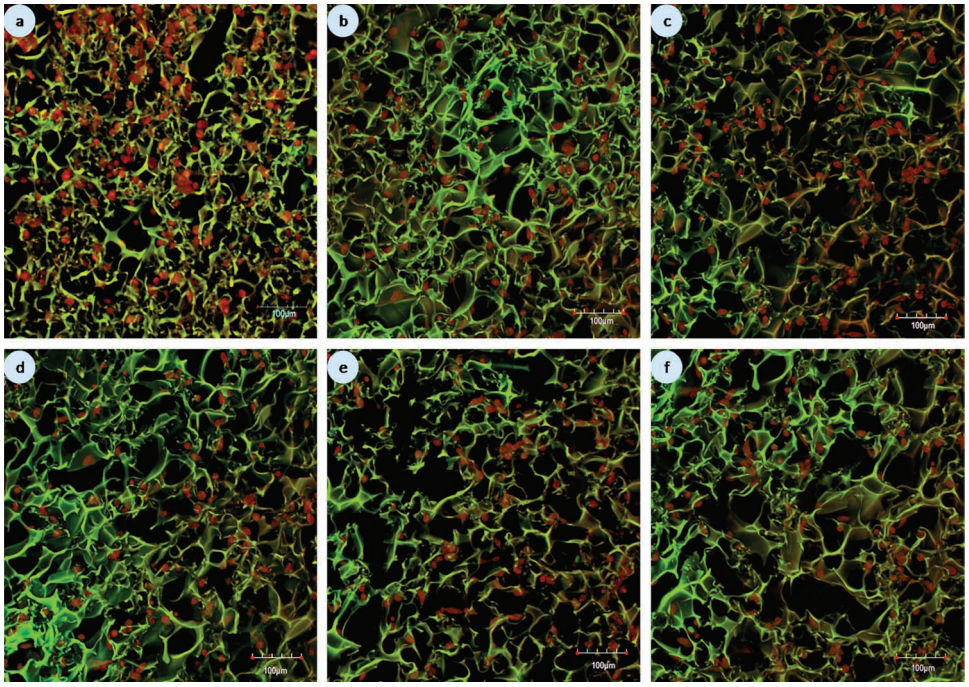

Figure 8. Morphology of MDA-MB-231 human breast adenocarcinoma cells 2% *A. mylitta* silk fibroin scaffolds a) untreated, b) treated with Paclitaxel (50 ± 0.17 μM), c) Celecoxib (934 μM), d) ZD6474 (25 μM), e) a combination of Paclitaxel (50 μM) with Celecoxib (934 μM), and f) ca ombination of Paclitaxel (50 μM) with ZD6474 (25 μM). The cells were stained with rhodamine-phalloidin for actin filaments (red) and Hoechst 33342 for nuclei (green). Images were taken from the mid-peripheral region of the constructs in all the cases. Scale bars represent 100 μm.

excess stained was washed off. Sections were cut and visualized under Nikon Stereozoom microscope (SMZ1500).

Chemotherapeutic Drug Studies: The IC_{50} of paclitaxel, Celecoxib and ZD6474 for the cells grown in 2D and 3D were calculated separately. Cell viability was assayed by MTT assay to determine the activity of anti-cancer drugs. Cell viability of drug treated and untreated MDA-MB-231 cells was measured using a Live/Dead viability/cytotoxicity kit (Molecular Probes, USA) using the manufacturer's protocol. Equal numbers of cells (10^6) were seeded on each scaffold. Cells were trypsinized counted with help of a haemocytometer and 10^5 cells were seeded on 24-well plates containing *A. mylitta* fibroin scaffolds. The required number of cells were suspended in a volume of 20 μl. 10 μl of this suspension was seeded on the top surface of the scaffolds, with 2 μl at 4 peripheral points, and 2 ul at the central point. These cells were allowed to attach for a 3 h at 37 °C and 5% CO_2. The scaffolds were turned over and the rest of 10 μl suspension was seeded in a similar fashion. The cultures were incubated for 7 days in a humidified atmosphere containing 5% CO_2 at 37 °C. The drug treated samples were serum starved for 24 h, and then treated with drugs for 48 h. Cells were incubated in 40 nm calcein AM, 20 nM ethidium homodimer in DMEM minus FBS for 15 min in the dark. Samples were analyzed by confocal FV 1000 Advance software v. 4.1 (Olympus) with 494 nm and 527 nm excitation, to visualize calcein stained live cells and ethidium homodimer stained dead cells.

Expression of MMP-2 and MMP-9 in Drug Treated and Untreated Cultures: MMP-2 and MMP-9 enzymatic activity in drug treated and untreated seeded scaffolds were analyzed by SDS-PAGE gelatin zymography as described earlier.[49] Briefly, the constructs were serum starved, treated with drugs for 48 h and conditioned media of both treated and untreated constructs, normalized to an equal amount of protein (40 μg), was electrophoresed in the absence of a reducing agent in 10% SDS-PAGE containing 0.2% (w/v) gelatin. Collagenase (Sigma) was used as a positive control. Gels were washed in a renaturating buffer (1% Triton X-100) at room temperature for 20 min, and then incubated at 37 °C overnight in a buffer containing 10 mM $CaCl_2$, 0.15 M NaCl, and 50 mM Tris (pH 7.5). The gels were stained with 0.5% Coomassie Blue, and enzyme activity was detected as clear, white bands. The images were analyzed by Image J (NIH) software.

VEGF and IL-8 Production by Drug Treated and Untreated Cancer Cultures: The amount of VEGF and IL-8 present in the media samples was determined using the Assay Kit from R&D systems. Briefly, the cell culture supernatant was collected, centrifuged, added to the Elisa plate well containing the assay diluent and incubated for 2 h at room temperature. After washing the excess sample, the conjugate was added and incubated for 2 h (for VEGF) or 1 h (for IL-8) at room temperature. After washing the conjugate was added and again the plate was incubated for 20–30 min at room temperature. After addition of stop solution the OD was determined to analyze the VEGF and IL-8 content. The readings were taken at 540 nm and subtracted from readings at 450 nm to remove the background.

Confocal Laser Microscopy and Morphology of Cells: Attachment, spreading and morphology of MDA-MB-231 cells on *A. mylitta* silk fibroin scaffolds was assessed using confocal microscopy. For long-term cell culture study, *A. mylitta* silk fibroin scaffold were seeded with MDA- MB-231 cells at the density of 3×10^6 cells per scaffold and cultured for 60 days. For chemotherapy studies, 10^6 cells were seeded on *A. mylitta* silk fibroin scaffolds and 6-well plates coated with and without *A. mylitta* silk fibroin. The cultures were maintained at 37 °C in a humidified 95% air/5% CO_2 in DMEM medium with 10% FBS (Gibco). The culture medium was replaced every 3 days. The cells were fixed in 4% paraformaldehyde for 15 min, then treated with 0.2% Triton X-100 in PBS for 15 min to permeabilise the membranes. Actin microfilaments were then stained with Rhodamine-phalloidin (0.8U/mL; Molecular Probes, USA) and nuclei were stained using Hoechst 33342 (5 μg/ml; Molecular Probes, USA). The constructs were imaged by using a confocal laser scanning microscope (CLSM, Olympus FV 1000 attached with inverted microscope IX 81, Japan) with Argon (488 nm) and HeNe

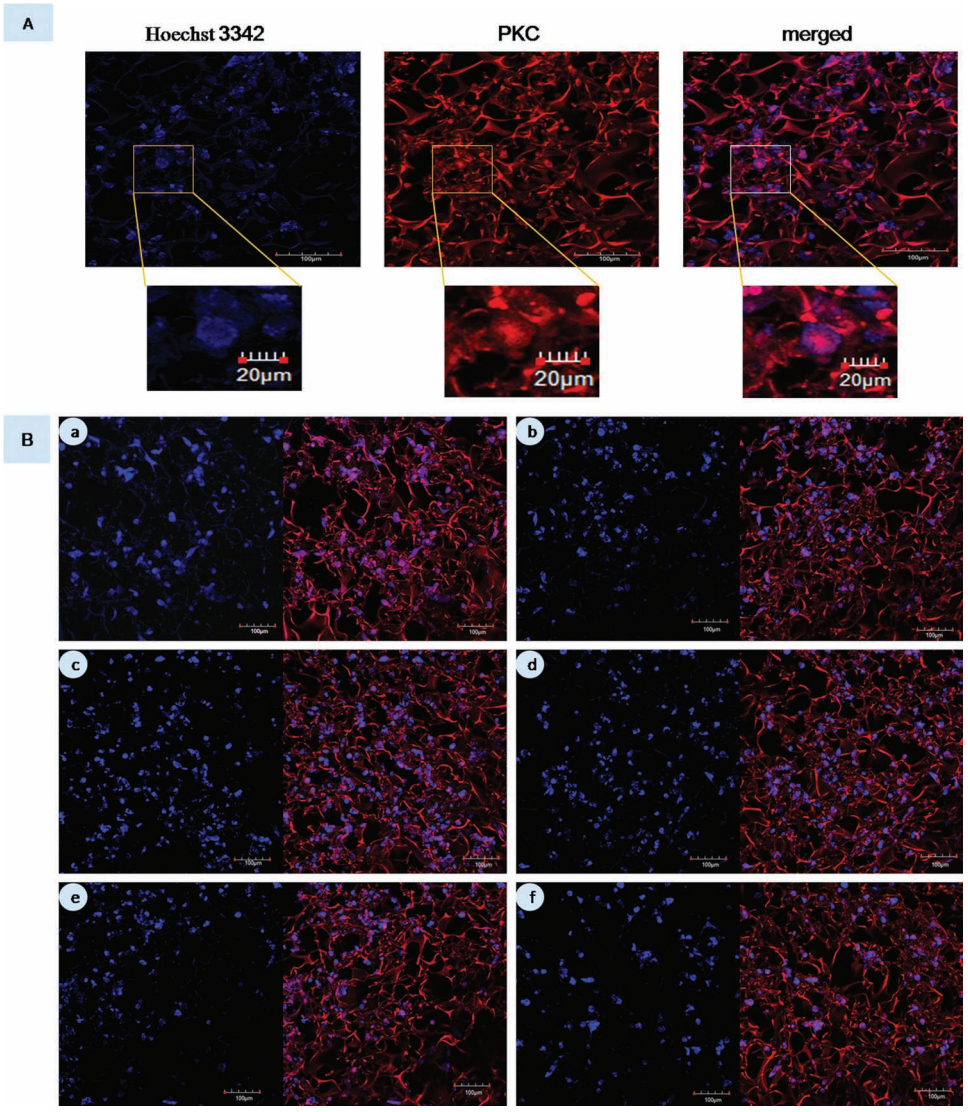

Figure 9. A) Confocal microscopy images showing nuclear localization of PKC. Scale bars represent 20 μm. B) Confocal microscopy images showing nuclear (stained with Hoechst 33342) and merged immunostaining of cells against PKC (stained with TRITC-conjugated secondary antibodies) under a) untreated and b–f) drug treated conditions. Drugs used were b) Paclitaxel (50 μM), c) Celecoxib (934 μM), d) ZD6474 (25 μM), e) a combination of Paclitaxel (50 μM) with Celecoxib (934 μM), and f) a combination of Paclitaxel (50 μM) with ZD6474 (25 μM). Immunostaining of constructs against PKC revealed higher expression of PKC visualized as pink areas in the blue nuclei of untreated tissue constructs when compared to treated samples. Scale bars represent 100 μm.

(534 nm) lasers. 2D multichannel image processing was carried out by FV 1000 Advance software version 4.1 (Olympus, Japan).

Immunofluorescence, Microscopy, and Image Analysis: Antibodies were purchased from Santa Cruz Biotechnology, USA. The constructs were stained with primary antibody against PKC (rabbit polyclonal IgG antibody, 1:100) in 1% BSA in PBS for 1 h and washed thoroughly with PBS. Then they were incubated in secondary antibody (goat anti-rabbit antibody conjugated with TRITC, 1:2000) for 1 h. The constructs were washed and counterstained with Hoechst 33342. Confocal images were acquired and stacked using confocal laser scanning microscope. Images were processed and stacked by FV 1000 Advance software version 4.1 (Olympus, Japan). The images were then analyzed by Image J (NIH) software.

Statistical Analysis: All quantitative experiments were run in quadruplicate and the results are expressed as means ± standard deviation for n = 4, unless indicated otherwise. The glucose and lactate assay results are expressed as means ± standard deviation for n = 3. Statistical analysis of the data was performed by one-way analysis of variance (ANOVA) and Students t-test. Differences between groups at a level of $P \leq 0.05$ were considered as statistically significant and those at $P < 0.01$ as highly significant.

Supporting Information

Supporting Information is available from the Wiley Online Library or from the author.

Acknowledgements

This work is supported by Department of Biotechnology and its Bioinformatics facilities, Department of Science and Technology,

Government of India. The authors would also like to thank Dr. Mahitosh Mandal (School of Medical Science and Technology, Indian Institute of Technology Kharagpur) for providing us with the drugs Celecoxib and ZD6474. The authors are thankful to the Indian Council of Medical Research and its experts for valuable scientific discussion/suggestions.

Received: February 7, 2012
Revised: April 11, 2012
Published online: July 3, 2012

[1] D. H. Kim, D. Wirtz, *Proc. Natl. Acad. Sci. USA* **2011**, *108*, 6693.
[2] E. M. Lawler, F. R. Miller, G. H. Heppner, *In Vitro* **1983**, *19*, 600.
[3] M. J. Bissell, P. A. Kenny, D. C. Radisky, *Cold Spring Harb. Symp. Quant. Biol.* **2005**, *70*, 343.
[4] K. M. Yamada, E. Cukierman, *Cell* **2007**, *130*, 601.
[5] T. Jacks, R. A. Weinberg, *Cell* **2002**, *111*, 923.
[6] S. I. Fraley, Y. Feng, R. Krishnamurthy, D. H. Kim, A. Celedon, G. D. Longmore, D. Wirtz, *Nat. Cell Biol.* **2010**, *12*, 598.
[7] P. A. Kenny, G. Y. Lee, C. A. Myers, R. M. Neve, J. R. Semeiks, P. T. Spellman, K. Lorenz, E. H. Lee, M. H. Barcellos-Hoff, O. W. Petersen, J. W. Gray, M. J. Bissell, *Mol. Oncol.* **2007**, *1*, 84.
[8] J. Lee, M. J. Cuddihy, N. A. Kotov, *Tissue Eng. Part B Rev.* **2008**, *14*, 61.
[9] C. Feder-Mengus, S. Ghosh, A. Reschner, I. Martin, G. C. Spagnoli, *Trends Mol Med.* **2008**, *14*, 333.
[10] D. E. Ingber, *Semin. Cancer Biol.* **2008**, *18*, 356.
[11] E. Burdett, F. K. Kasper, A. G. Mikos, J. A. Ludwig, *Tissue Eng. Part B Rev.* **2010**, *16*, 351.
[12] M. J. Bissell, D. Radisky, *Nat. Rev. Cancer* **2001**, *1*, 46.
[13] T. Jacks, R. A. Weinberg, *Cell* **2002**, *111*, 923.
[14] M. M. Mueller, N. E. Fusenig, *Nat. Rev. Cancer* **2004**, *4*, 839.
[15] N. Zahir, V. M. Weaver, *Curr. Opin. Genet. Dev.* **2004**, *14*, 71.
[16] T. Roose, S. J. Chapman, P. K. Maini, *Siam Rev.* **2007**, *49*, 179.
[17] E. Cukierman, R. Pankov, K. M. Yamada, *Curr. Opin. Cell Biol.* **2002**, *14*, 633.
[18] M. Bissell, *Nature* **2003**, *424*, 870.
[19] J. Erler, V. Weaver, *Clin. Exp. Metastasis* **2009**, *26*, 35.
[20] B. E. Miller, F. R. Miller, G. H. Heppner, *Cancer Res.* **1985**, *45*, 4200.
[21] D. W. Hutmacher, *Nat. Mater.* **2010**, *9*, 90.
[22] K. J. Martin, D. R. Patrick, M. J. Bissell, M. V. Fournier, *PLoS One* **2008**, *3*, e2994.
[23] J. L. Inman, M. J. Bissell, *J. Biol.* **2010**, *9*, 2.
[24] S. K. Muthuswamy, *Breast Cancer Res.* **2011**, *13*, 103.
[25] L. Li, Y. Lu, *J. Cancer* **2011**, *2*, 458.
[26] J. Koivunen, V. Aaltonen, J. Peltonen, *Cancer Lett.* **2006**, *235*, 1.
[27] J. E. Rundhaug, *J. Cell Mol. Med.* **2005**, *9*, 267.
[28] L. M. Coussens, B. Fingleton, L. M. Matrisian, *Science* **2002**, *295*, 2387.
[29] M. Egeblad, Z. Werb, *Nat. Rev. Cancer* **2002**, *2*, 161.
[30] E. I. Deryugina, J. P. Quigley, *Cancer Metastasis Rev.* **2006**, *25*, 9.
[31] A. Page-McCaw, A. J. Ewald, Z. Werb, *Nat. Rev. Mol. Cell Biol.* **2007**, *8*, 221.
[32] A. Beliveau, J. D. Mott, A. Lo, E. I. Chen, A. A. Koller, P. Yaswen, J. Muschler, M. J. Bissell, *Genes Dev.* **2010**, *24*, 2800.
[33] A. R. Nelson, B. Fingleton, M. L. Rothenberg, L. M. Matrisian, *J. Clin. Oncol.* **2000**, *18*, 1135.
[34] M. S. Woo, S. H. Jung, S. Y. Kim, J. W. Hyun, K. H. Ko, W. K. Kim, H. S. Kim, *Biochem. Biophys. Res. Commun.* **2005**, *335*, 1017.
[35] F. Tas, D. Duranyildiz, H. Oguz, H. Camlica, V. Yasasever, E. Topuz, *Cancer Invest.* **2006**, *24*, 492.
[36] G. Gasparini, *Crit. Rev. Oncol/Hematol.* **2001**, *37*, 3.
[37] D. Chelouche-Lev, C. P. Miller, C. Tellez, M. Ruiz, M. Bar-Eli, J. E. Price, *Eur. J. Cancer* **2004**, *40*, 2509.
[38] J. H. Harmey, D. Bouchier-Hayes, *BioEssays* **2002**, *24*, 280.
[39] D. J. Price, T. Miralem, S. Jiang, R. Steinberg, H. Avraham, *Cell Growth Differ.* **2001**, *12*, 129.
[40] M. Bar-Eli, *Pathobiology* **1999**, *67*, 3.
[41] A. J. Ryan, S. R. Wedge, *Br. J. Cancer* **2005**, *92*, S6.
[42] B. C. Moore, D. L. Simmons, *Curr. Med. Chem.* **2000**, *7*, 1131.
[43] M. Sahin, E. Sahin, S. Gümüslü, *Angiology* **2009**, *60*, 242.
[44] A. Jordan, J. A. Hadfield, N. J. Lawrence, A. T. McGown, *Med. Res. Rev.* **1998**, *18*, 259.
[45] G. T. Reeves, S. E. Fraser, *PLoS Biol.* **2009**, *7*, e21.
[46] C. Acharya, S. K. Ghosh, S. C. Kundu, *J. Mater. Sci. Mater. Med.* **2008**, *19*, 2827.
[47] B. B. Mandal, S. C Kundu, *Biomaterials* **2009**, *30*, 2956.
[48] B. B. Mandal, S. C. Kundu, *Acta Biomater.* **2009**, *5*, 2579.
[49] S. Talukdar, M. Mandal, D. W. Hutmacher, P. J. Russell, C. Soekmadji, S. C. Kundu, *Biomaterials* **2011**, *32*, 2149.
[50] J. J. Casciari, S. V. Sotirchos, R. M. Sutherland, *Cell Prolif.* **1992**, *25*, 1.
[51] Y. Kim, M. A. Stolarska, H. G. Othmer, *Prog. Biophys. Mol. Biol.* **2011**, *106*, 353.
[52] C. C. Park, M. J. Bissell, M. H. Barcellos-Hoff, *Mol. Med. Today* **2000**, *6*, 324.
[53] C. C. Fischbach, R. Chen, T. Matsumoto, T. Schmelzle, J. S. Brugge, P. J. Polverini, D. J. Mooney, *Nat. Methods* **2007**, *4*, 855 .
[54] A. Starzec, D. Briane, M. Kraemer, J. C. Kouyoumdjian, J. L. Moretti, R. Beaupain, O. Oudar, *Biol. Cell* **2003**, *95*, 257.
[55] D. Loessner, K. S. Stok, M. P. Lutolff, D. W. Hutmacher, J. A. Clements, S. C. Rizzi, *Biomaterials* **2010**, *31*, 8494.
[56] Y. Dong, O. L. Tan, D. Loessner, C. Stephens, C. Walpole, G. M. Boyle, P. G. Parsons, J. A. Clements, *Cancer Res.* **2010**, *70*, 2624.
[57] A. W. Johnson, B. Harley, *Anticancer Res.* **2011**, *31*, 3237.
[58] C. D. Bortner, J. A. Cidlowski, *Cell Death Differ.* **2002**, *9*, 1307.
[59] S. A. Lee, J. W. Karaszkiewicz, W. B. Anderson, *Cancer Res.* **1992**, *52*, 3750.
[60] G. C. Blobe, L. M. Obeid, Y. A. Hannun, *Cancer Metastasis Rev.* **1994**, *13*, 411.
[61] H. Yoshiji, S. Kuriyama, D. K. Ways, J. Yoshii, Y. Miyamoto, M. Kawata, Y. Ikenaka, H. Tsujinoue, T. Nakatani, M. Shibuya, H. Fukui, *Cancer Res.* **1999**, *59*, 4413.
[62] H. Xiao, X. H. Bai, A. Kapus, W. Y. Lu, A. S. Mak, M. Liu, *Mol. Cell Biol.* **2010**, *30*, 5545.
[63] S. Talukdar, Q. T. Nguyen, A. C. Chen, R. L. Sah, S. C. Kundu, *Biomaterials* **2011**, *32*, 8927.